Transient DC Bias and Current Impact Effects of High-Frequency-Isolated Bidirectional DC–DC Converter in Practice

Biao Zhao, *Member, IEEE*, Qiang Song, *Member, IEEE*, Wenhua Liu, and Yuming Zhao

***Abstract*—This paper presents the transient dc bias and the current impact effects of a high-frequency-isolated bidirectional dc–dc converter (IBDC) in practice because the theoretical premise in the steady process cannot be satisfied strictly in the transient process. The transient characterizations of IBDC under the steady phase-shift (SPS) strategy are analyzed comprehensively, and the corresponding model is modified for all of the transient processes in the same and different power flows. Due to the existence of the dc bias, the current model in the transient process is different from the traditional model in the steady process, and the models are different with different operating conditions. On this basis, a transient phase-shift (TPS) strategy is proposed to improve the transient performance of the SPS strategy. Unlike in the SPS strategy, the voltages of the transformer are symmetrical in the TPS strategy, which causes that the voltage–time product of the transformer voltages is zero during a switching period, then eliminates the transient dc bias and improves the current impact, and further increases the response speed of the transient process effectively. Finally, comprehensive experiments verify the theoretical analysis.**

***Index Terms*—Current impact, dc bias, dc–dc converter, dual-active-bridge (DAB), high-frequency-link (HFL), phase-shift (PS), transient.**

I. Introduction

ISOLATED bidirectional dc/dc converters (IBDCs) can not only realize dc voltage conversion and galvanic isolation, but also realize the bidirectional power transmission, which has wide application prospects in the energy storage system, uninterruptible power system, dc distribution system, etc. [1]–[5]. Moreover, a high-frequency (HF)-isolated transformer can be employed in IBDCs instead of the line-frequency transformer to provide the voltage matching and galvanic isolation, which can significantly reduce weight and volume, as well as improve the power density of the system. Dual-active-bridge (DAB) is a promising HF IBDC structure, and attracts increasing attention because of its advantages of high power density, zero-voltage switching, fast dynamic response, bidirectional power transfer capability, modularity, and symmetric structure [6]–[8].

Manuscript received November 10, 2014; revised May 1, 2015; accepted June 5, 2015. Date of publication June 16, 2015; date of current version November 30, 2015. This work was supported by the National High Technology Research and Development (863) Program of China under Grant 2013AA050104. Recommended for publication by Associate Editor T.-J. Liang. *(Corresponding author: Qiang Song.)*

B. Zhao, Q. Song, and W. Liu are with the Department of Electrical Engineering, Tsinghua University, Beijing 100084, China (e-mail: zhaobiao@tsinghua.edu.cn; songqiang@tsinghua.edu.cn; liuwenh@tsinghua.edu.cn).

Y. Zhao is with Shenzhen Power Supply Corporation, Shenzhen 518048, China (e-mail: zhaoym97@sina.com).

Color versions of one or more of the figures in this paper are available online at http://ieeexplore.ieee.org.

Digital Object Identifier 10.1109/TPEL.2015.2445831

So far, most of the international research on DAB has focused on the following aspects: basic characterization, topology and soft-switching solution, control strategy, and hardware design and optimization [8]. The basic characteristics, such as transmission power characterization, dead-time effect, and dynamic model, have been studied in [6], [9]–[12]. Many new topologies and soft-switching solutions have also been proposed to increase soft-switching range and to improve efficiency [13]–[15]. A family of multiple control algorithms, especially the optimized phase-shift (PS) control, has been analyzed to improve the characteristics of the circulating current, enhance power transmission capacity, and so on [16]–[18]. The optimized design of parameters, magnetic components (transformer and inductor), power devices, and hardware structure has also been investigated to increase the power density, flexibility, and reliability of the converter [19]–[21]. All of these studies can contribute to improving the DAB performance and to promoting DAB application.

However, the dc bias characteristic is seldom mentioned. In fact, in previous theoretical analyses, the assumption that the voltage–time product of the transformer voltage is zero during a switching period is usually admitted [6]–[21]. Based on this premise, there is no dc bias in the transformer current. In practice, however, this premise cannot be satisfied strictly. The factors that can interrupt the premise in practical are as follows: 1) the inconsistency between the characteristic parameters of the switches, such as on-state voltage drop, switching speed, etc.; 2) the inconsistency of the pulse width from the driving control circuit; 3) the variation in the terminal dc voltage during a period; and 4) the adjustment of the PS ratio derived from the closed-loop control system. Therefore, the dc bias becomes a practical issue because of the inconsistency between theory and practice. This problem affects the high-frequency-link (HFL) current, especially in the transient process. In fact, different from the traditional bidirectional converter, the HFL current of DAB is the most key element to control the direction and magnitude of power flow, and the transient dc bias and the impact of the HFL current essentially render the DAB unreliable and prone to failure during startup and power switching.

As for the factor 1, try the best to build the hardware based on the switches with consistent static and dynamic characteristics, such as switches obtained from the same batches produced by the same manufacturer, the intelligent power module with multiple switches, etc. As for the factor 2, the inconsistency in driving pulse width is decided by the unmatched delays in the hardware and in the accuracy of the controller. This influence

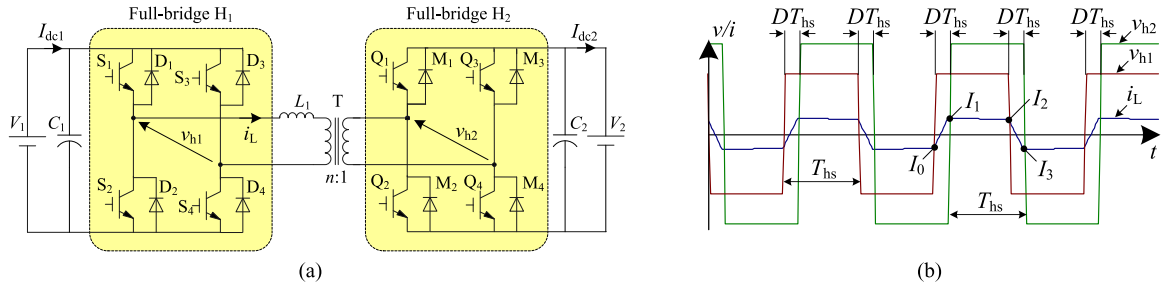

Fig. 1. PS principle of DAB. (a) Topology. (b) HFL voltage and current of PS control in steady state.

can be disregarded by using driving components obtained from the same batches produced by the same manufacturer and with a fast and precise control chip. As for the factor 3, because the operating current of DAB is in HF status, so the ripple of the terminal dc voltage is small with a suitable dc capacitor and modulation method. This ripple has little effect on the voltage–time product during one switching period. The asymmetry of the voltage–time product as a result of factor 4 is more serious than the effects of the first three factors. This asymmetry is determined by the nature control rule and cannot be improved simply by optimizing the design of the hardware.

The flux balancing problems of the isolation transformer because of the nonideal behavior of the semiconductor switches and the pulsating-dc voltage were discussed in [22] and [23], but the transient dc bias and the impact effects attributed to PS control were not analyzed. The over current effect and transient response caused by the dc component of the current were concerned in [24] and [25], but the influence mechanism is not investigated and the characterizations of the dc bias with different operation conditions are not analyzed comprehensively.

According to the previous discussion, this paper presents a comprehensive theoretical analysis and experimental verification of the transient dc bias and of the current impact effects, and on this basis, a transient PS updating strategy is proposed to eliminate the dc bias and to improve the current impact effect.

II. Transient DC Bias and Current Impact in Practice

A. PS Principle of DAB

Fig. 1 shows the PS operation principle of DAB. Similar to the power control in traditional ac power systems, the direction and magnitude of power flow of DAB can also be controlled by adjusting the PS ratio *D* between the ac output voltages v_{h1} and v_{h2} of bridges H_1 and H_2. However, the voltages at both sides of the inductor are line-frequency sinusoidal waves in traditional ac power system, whereas these voltages are HF square waves in DAB.

The power of DAB flows from the leading square wave to the lagging square wave, that is the power flows from the V_1 side to the V_2 side when $D \geq 0$ and from the V_2 side to the V_1 side when $D<0$. From [18], the current expressions of HFL can be derived as indicated in Table I at different flow directions. In Fig. 1 and Table I, L is the sum of the inductance of the series auxiliary inductor and the leakage inductance of the HF transformer; n is the transformer turn ratio; V_1 and V_2 are dc terminal voltages

TABLE I
Peak Current of DAB With PS Control

D	$I_0/[nV_2/(4f_sL)]$	$I_1/[nV_2/(4f_sL)]$	$I_2/[nV_2/(4f_sL)]$	$I_3/[nV_2/(4f_sL)]$
$D \geq 0$	$1–k–2D$	$1–k+2Dk$	$k–1+2D$	$k–1–2Dk$
$D < 0$	$1–k+2\|D\|k$	$1–k–2\|D\|$	$k–1–2\|D\|k$	$k–1+2\|D\|$

of DAB; v_{h1} and v_{h2} are the ac output voltages of H_1 and H_2, respectively; i_L is the current of inductor L; T_{hs} is a half-switching period, $f_s = 1/(2T_{hs})$ is switching frequency, and D is the PS ratio in the half-switching period; where $0 \leq D \leq 1$ and $k = V_1/nV_2$ is the voltage conversion ratio.

B. Transient DC Bias and Current Impact in Practice

As shown in Fig. 1, the voltage–time product of the transformer voltages is zero during a switching period when PS ratio is constant. Based on this premise, the transformer current does not contain a dc bias. However, the premise cannot be satisfied in practice, especially in the transient process.

Fig. 2 shows the transient waveforms of the DAB in practice, which are measured with a 500 MHz mixed signal oscilloscope. At $t = t_0$, the DAB is activated, and the PS ratio is increased from 0 to *D*. It can be seen that there is a transient impact and dc bias phenomenon in the HFL current. The average value of the HFL current is changed to $I_{T\mathrm{dc}}$ and the maximum value is also changed to I_M. These changes induce considerable current impact on the switches and compromise the safe operation of the converter. The DAB current is in the HF and the phenomenon mainly occurs during the transient state; hence, it is often overlooked in practice, as shown in Fig. 2(a). In fact, the transient dc bias and current impact are the key factors in the unreliability of DAB and its proneness to failure during startup and power switching.

In this paper, we define the PS control discussed in Fig. 1 as steady-phase-shift (SPS).

III. Transient Characterization of the SPS Updating Strategy

A. Transient Characterization With a Constant Power Flow

In this paper, the forward power flow is from the V_1 side to the V_2 side and the reverse power flow is from the V_2 side to the V_1 side. Thus, the leading voltages in the forward and reverse power flows are v_{h1} and v_{h2}, respectively; the polarities of the

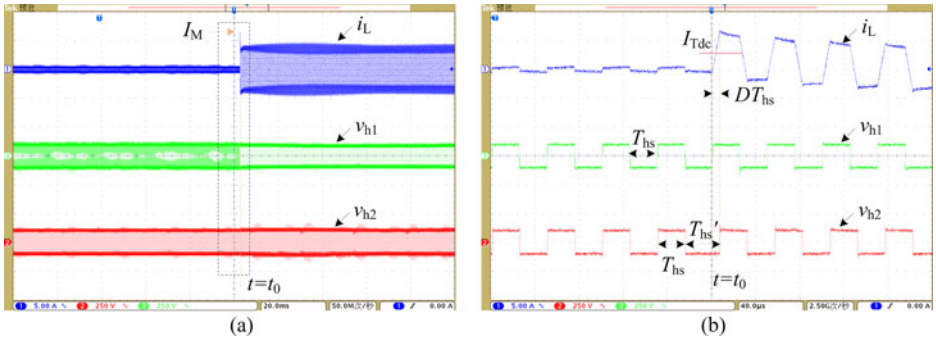

Fig. 2. Transient dc bias and current impact effect in practice. (a) Transient waveforms. (b) Enlarged waveforms.

PS ratios in the forward and reverse power flows are positive and negative, respectively. Here, take the forward power flow as example to analyze, and the reverse power flow can be analyzed similarly.

1) Increase in Power: PS ratio increases when the power increases, that is $0 \le D_1 < D_2$. The transient waveforms of DAB under the SPS updating strategy are shown in Fig. 3(a). In the first switching period *ST1*, $\Delta t_1 = D_1 T_{hs}$; in the second switching period *ST2*, $\Delta t_2 = D_2 T_{hs}$. Then, we have

$$T_{\rm hs}{}' = T_{\rm hs} + \Delta t_2 - \Delta t_1 = (1 + D_2 - D_1)\, T_{\rm hs} > T_{\rm hs}. \quad (1)$$

From (1), the transformer voltages at the primary and secondary sides are asymmetrical during the transient process. As a result, the voltage–time product of the transformer voltages is nonzero during a switching period, so the dc bias $I_{T\rm dc}$ occurs in transient process.

According to Table I and Fig. 3(a), we have

$$\begin{cases} i_L(t_0) = \dfrac{nV_2}{4f_sL}(1 - k - 2D_1) \\ i_L(t_1) = i_L(t_0) + \dfrac{V_1 + nV_2}{L}\Delta t_2 \\ i_L(t_2) = i_L(t_1) + \dfrac{V_1 - nV_2}{L}(T_{\rm hs} - \Delta t_2) \\ i_L(t_3) = i_L(t_2) + \dfrac{-V_1 - nV_2}{L}\Delta t_2 \\ i_L(t_4) = i_L(t_3) + \dfrac{-V_1 - nV_2}{L}(T_{\rm hs} - \Delta t_2). \end{cases} \quad (2)$$

From (2), the HFL peak currents can be derived

$$\begin{cases} I_1 = \dfrac{nV_2}{4f_sL}[1 - k - 2D_1 + 2D_2(k+1)] \\ I_2 = \dfrac{nV_2}{4f_sL}(k - 1 - 2D_1 + 4D_2) \\ I_3 = \dfrac{nV_2}{4f_sL}[(k-1)(1-2D_2) - 2D_1] \\ I_4 = \dfrac{nV_2}{4f_sL}(1 - k - 2D_1). \end{cases} \quad (3)$$

Then, the dc bias $I_{T\rm dc}$ can be derived

$$I_{T\rm dc} = \frac{I_1 + I_3}{2} = \frac{nV_2}{4f_sL}[2(D_2 - D_1)]. \quad (4)$$

Because of the existence of the dc bias phenomenon, the HFL current increases in the transient process which causes great current impact I_1 or I_2 on the switches and endangers the safe operation of the converter. Furthermore, the transient dc bias in this situation is mainly related to the increment (D_2–D_1) of the PS ratio.

2) Decrease in Power: The PS ratio decreases when the power decreases, that is $0 \le D_2 < D_1$. The transient waveforms of DAB under the SPS updating strategy are shown in Fig. 3(b). In the first switching period *ST1*, $\Delta t_1 = D_1 T_{hs}$; in the second switching period *ST2*, $\Delta t_2 = D_2 T_{hs}$. Then, we have

$$T'_{\rm hs} = T_{\rm hs} + \Delta t_2 - \Delta t_1 = (1 + D_2 - D_1)\, T_{\rm hs} < T_{\rm hs}. \quad (5)$$

Similar to the last situation, the transformer voltages are also asymmetrical when the PS ratio decreases. Moreover, the dc bias remains. Unlike in the transient process with $0 \le D_1 < D_2$, the maximum value of the HFL current with $0 \le D_2 < D_1$ in *ST2* is smaller than that in *ST1* because the power decreases. Therefore, this current remains within the safe area of the converter. However, the HFL peak current also increases, unlike the steady state mentioned in Section II-A. That is the $max\{|I_1|,|I_2|,|I_3|,|I_4|\}$ in Fig. 3(b) is higher than that in Fig. 1(b) with the same PS ratio.

According to Table I and Fig. 3(b), the expressions of the HFL peak currents and dc bias with the decrease in PS ratio can be derived as the same with (3) and (4). However, the transient dc bias with the decrease in PS ratio is mainly related to the decrement (D_2–D_1) of the PS ratio because $0 \le D_2 < D_1$ as per (4). This situation differs from the increment in the situation with the increase of the PS ratio. Moreover, from Fig. 3(b), the polarities of the transient dc bias and of current impact changes from positive to negative.

Similar to $0 \le D_1 < D_2$ in the forward power flow, the dc bias and current impact effects are induced when $D_2 < D_1 \le 0$ in the reverse power flow. However, the polarities of the transient dc bias and of current impact shift from positive to negative. Moreover, the transient dc bias is mainly related to the decrement ($|D_1|$–$|D_2|$) of the PS ratio. Correspondingly, the polarities of the transient dc bias and of current impact shift from negative to positive when $D_1 < D_2 \le 0$, the bias is mainly related to the increment ($|D_1|$–$|D_2|$) of the PS ratio.

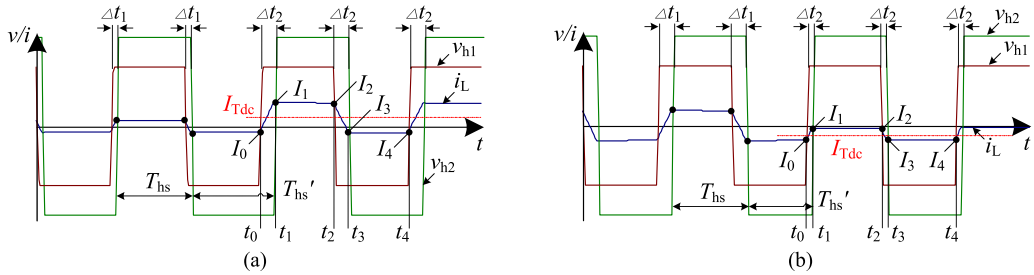

Fig. 3. Transient waveforms under the SPS updating strategy with a constant power flow. (a) Increase in power. (b) Decrease in power.

B. Transient Characterization With Different Power Flows

When the direction of the power flow changes, the polarity of the PS ratio also shifts.

1) Reverse to Forward Power Flow: When the power flow changes from the reverse to the forward direction, the polarity of the PS ratio shifts from negative to positive, that is $D_1 < 0 < D_2$. The transient waveforms of DAB under the SPS updating strategy are shown in Fig. 4(a). Unlike the situation under a constant power flow direction, the phase of v_{h2} is fixed and that of v_{h1} changes to control the PS ratio in *ST1*. However, the control status is changed in *ST2* such that the phase of v_{h1} is fixed and that of v_{h2} changes to control the PS ratio.

In the first switching period *ST1*, $\Delta t_1 = |D_1|T_{hs}$. In the second switching period *ST2*, $\Delta t_2 = D_2 T_{hs}$. At t_0, the second period begins, the PS ratio changes from negative to positive, and v_{h1} shifts to positive immediately. We have

$$\begin{cases} T'_{\rm hs} = T_{\rm hs} - \Delta t_1 = (1 - |\,D_1|)\,T_{\rm hs} < T_{\rm hs} \\ T''_{\rm hs} = T_{\rm hs} + \Delta t_2 = (1 + |\,D_2|)\,T_{\rm hs} > T_{\rm hs}. \end{cases} \tag{6}$$

From (6), in the transient process, the transformer voltages are also asymmetrical at the primary and secondary sides. The voltage–time product of the transformer is nonzero during a switching period; thus, the dc bias $I_{T\rm dc}$ occurs in this process.

According to Table I and Fig. 4(a), the HFL peak currents can be derived

$$\begin{cases} I_1 = \dfrac{nV_2}{4f_sL}\left[1 - k + 2|\,D_1|\,k + 2D_2\,(1+k)\right] \\ I_2 = \dfrac{nV_2}{4f_sL}\left(k - 1 + 2|\,D_1|\,k + 4D_2\right) \\ I_3 = \dfrac{nV_2}{4f_sL}\left[(k-1)\,(1-2D_2) + 2|\,D_1|\,k\right] \\ I_4 = \dfrac{nV_2}{4f_sL}\left(1 - k + 2|\,D_1|\,k\right). \end{cases} \tag{7}$$

Then, the dc bias $I_{T\rm dc}$ can be derived

$$I_{T\rm dc} = \frac{I_1 + I_3}{2} = \frac{nV_2}{4f_sL}\left[2\left(k|\,D_1| + D_2\right)\right]. \tag{8}$$

As in the scenario under a constant power flow direction, the dc bias and the current impact effects are induced given different power flow directions. However, the transient dc bias is mainly related to the nonstrict increment $(k|D_1| + |D_2|)$ of the PS ratio. In fact, Figs. 3 and 4 show that the current changes from negative to positive when $0 \le D_1 < D_2$, from positive to negative when $D_2 < D_1 \le 0$, and from positive to positive when $D_1 < 0 < D_2$ during Δt_2. Therefore, the transient dc bias and the current impact effects are enhanced when the power flow direction changes.

2) Forward to Reverse Power Flow: When the power flow shifts from the forward to the reverse direction, the polarity of the PS ratio changes from positive to negative, that is $D_2 < 0 < D_1$. The transient waveforms of DAB under the SPS updating strategy are shown in Fig. 4(b). Unlike in the situation with reverse to forward power flow, the phase of v_{h1} is fixed and the phase of v_{h2} changes to control the PS ratio in *ST1*. The control status is changed in *ST2* such that the phase of v_{h2} is fixed and the phase of v_{h1} changes to control the PS ratio.

In the first switching period *ST1*, $\Delta t_1 = D_1 T_{hs}$; in the second switching period *ST2*, $\Delta t_2 = |D_2|T_{hs}$. At t_0, the second period begins, the PS ratio shifts from positive to negative, and v_{h2} changes to positive immediately. We have

$$\begin{cases} T'_{\rm hs} = T_{\rm hs} + \Delta t_2 = (1 + |\,D_2|)\,T_{\rm hs} > T_{\rm hs} \\ T''_{\rm hs} = T_{\rm hs} - \Delta t_1 = (1 - |\,D_1|)\,T_{\rm hs} < T_{\rm hs}. \end{cases} \tag{9}$$

As in the previous situation, the transformer voltages are also asymmetrical and the dc bias remains. The HFL peak currents can thus be derived

$$\begin{cases} I_1 = \dfrac{nV_2}{4f_sL}\left[1 - k - 2D_1 - 2|\,D_2|\,(k+1)\right] \\ I_2 = \dfrac{nV_2}{4f_sL}\left(k - 1 - 2D_1 - 4|\,D_2|\,k\right) \\ I_3 = \dfrac{nV_2}{4f_sL}\left[k - 1 - 2D_1 + 2|\,D_2|\,(1-k)\right] \\ I_4 = \dfrac{nV_2}{4f_sL}\left(1 - k - 2D_1\right). \end{cases} \tag{10}$$

Then, the dc bias $I_{T\rm dc}$ can be derived

$$I_{T\rm dc} = \frac{I_1 + I_3}{2} = -\frac{nV_2}{4f_sL}\left[2\left(k|\,D_2| + D_1\right)\right]. \tag{11}$$

Similar to the previous situation, the transient dc bias and the current impact effects are more devastating than those with a constant power flow direction. However, the transient dc bias is mainly related to the nonstrict decrement $(k|D_2| + |D_1|)$ of the PS ratio, unlike $D_1 < 0 < D_2$. Furthermore, the polarity of $I_{T\rm dc}$ changes from positive to negative.

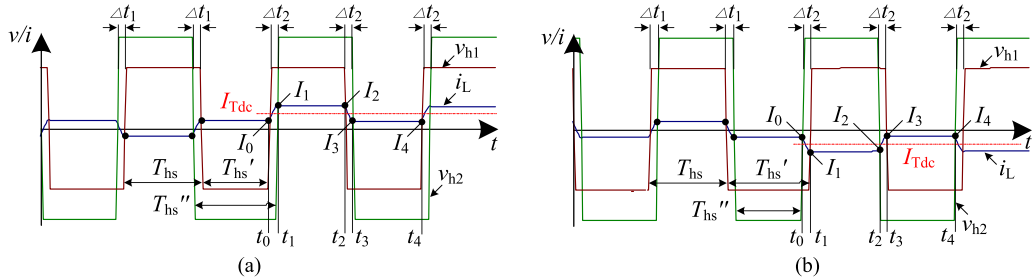

Fig. 4. Transient waveforms under the SPS updating strategy with different power flows. (a) Reverse to forward power flow. (b) Forward to reverse power flow.

TABLE II
MODIFIED MODEL OF PEAK CURRENT IN THE TRANSIENT PROCESS

Status	Power change	$I_1/[nV_2/(4f_sL)]$	$I_2/[nV_2/(4f_sL)]$	$I_3/[nV_2/(4f_sL)]$	$I_4/[nV_2/(4f_sL)]$
Constant flow	$P\uparrow$	$1–k–2D_1+2D_2(k+1)$	$k–1–2D_1+4D_2$	$(k–1)(1–2D_2)–2D_1$	$1–k–2D_1$
	$P\downarrow$				
Different flow	$-\rightarrow+$	$1-k+2\|D_1\|k+2D_2(k+1)$	$k–1+2\|D_1\|k+4D_2$	$(k–1)(1–2D_2)+2\|D_1\|k$	$1–k+2\|D_1\|k$
	$+\rightarrow-$	$1-k-2D_1–2\|D_2\|(k+1)$	$K–1–2D_1––4\|D_2\|k$	$k–1–2D_1+2\|D_2\|(1–k)$	$1–k–2D_1$

C. Modified Model of the Transient Process Under the SPS Updating Strategy

According to the previous analysis, Table II presents the modified model of HFL peak currents in the transient process under the SPS updating strategy. It can be seen that the HFL current model in the transient process differs from the traditional model of Table I under the steady process because of the dc bias.

With the same power flow, the HFL current increases when the power increases. As a result, a significant current impact is exerted on the switches and endangers the safe operation of the converter. When the power decreases, the HFL current remains within the safe area of the converter. However, compared to the steady state mentioned in Section II-A, the HFL current also increases. Moreover, the transient dc bias and current impact effects are more devastating under different power flows than under a constant power flow.

IV. IMPROVED TRANSIENT UPDATING STRATEGY

To decrease the transient dc bias and current impact, an improved transient updating strategy is proposed in this section; we defined it as the transient phase-shift (TPS) method.

A. Transient Characterization With a Constant Power Flow

In the forward power flow, the same scheme can be used for both power increase and decrease, as described in Fig. 3. The transient waveforms of DAB under the TPS updating strategy are shown in Fig. 5. The phase change for the lagging voltage v_{h2} is divided into two parts. These parts are added to the rising and falling edges of the lagging voltage during one period. In Fig. 5, $\Delta t_1 = D_1 T_{hs}$, $\Delta t_2 = D_2 T_{hs}$, $\Delta t_2{}' = D_2{}' T_{hs}$. Then, we have

$$\begin{cases} T_{\mathrm{hs0}}{}' = T_{\mathrm{hs}} + \Delta t_2' - \Delta t_1 = (1 + D_2' - D_1)\, T_{\mathrm{hs}} \\ T_{\mathrm{hs0}}{}'' = T_{\mathrm{hs}} - \Delta t_2' + \Delta t_2 = (1 - D_2' + D_2)\, T_{\mathrm{hs}}. \end{cases} \tag{12}$$

From (12), the asymmetrical period in (1) is divided into two parts. According to Table I and Fig. 5, we have

$$\begin{cases} i_L(t_0) = -\dfrac{nV_2}{4f_sL}\left[2D_1 - 1 + k\right] \\ i_L(t_1) = i_L(t_0) + \dfrac{V_1 + nV_2}{L}\Delta t_2' \\ i_L(t_2) = i_L(t_1) + \dfrac{V_1 - nV_2}{L}\left(T_{\mathrm{hs}} - \Delta t_2'\right) \\ i_L(t_3) = i_L(t_2) + \dfrac{-V_1 - nV_2}{L}\Delta t_2 \\ i_L(t_4) = i_L(t_3) + \dfrac{-V_1 - nV_2}{L}\left(T_{\mathrm{hs}} - \Delta t_2\right). \end{cases} \tag{13}$$

From (13), the HFL peak currents can also be derived

$$\begin{cases} I_1 = \dfrac{nV_2}{4f_sL}\left[1 - k - 2D_1 + 2(k+1)D_2'\right] \\ I_2 = \dfrac{nV_2}{4f_sL}\left(k - 1 - 2D_1 + 4D_2'\right) \\ I_3 = \dfrac{nV_2}{4f_sL}\left[k - 1 - 2D_1 + 4D_2' - 2D_2(k+1)\right] \\ I_4 = \dfrac{nV_2}{4f_sL}\left(1 - k - 2D_1 + 4D_2' - 4D_2\right). \end{cases} \tag{14}$$

Then, the dc bias $I_{T\mathrm{dc}}$ can be derived

$$I_{T\mathrm{dc}} = \frac{I_2 + I_4}{2} = \frac{nV_2}{4f_sL}(4D_2' - 2D_1 - 2D_2. \tag{15}$$

In order to eliminate the dc bias, we set $I_{T\mathrm{dc}} = 0$, from (15),

$$D_2' = \frac{D_1 + D_2}{2}. \tag{16}$$

Combine (12) and (16), we have

$$T_{\mathrm{hs0}}'' = T_{\mathrm{hs0}}' = \left(1 + \frac{D_2 - D_1}{2}\right) T_{\mathrm{hs}}. \tag{17}$$

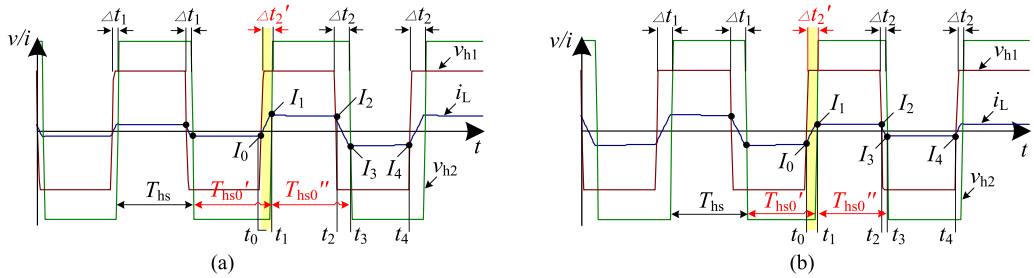

Fig. 5. Transient waveforms under the TPS updating strategy with constant power flow. (a) Increase in power. (b) Decrease in power.

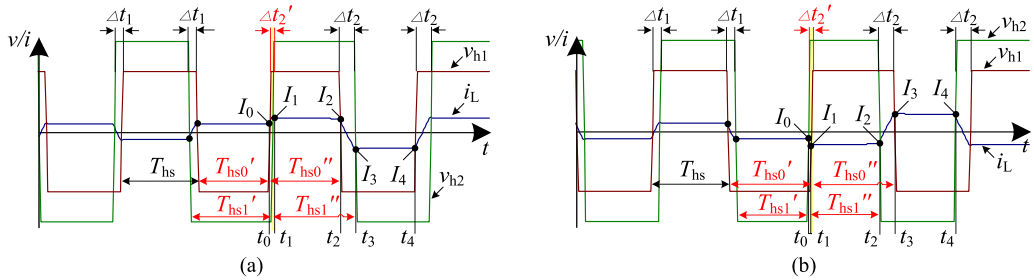

Fig. 6. Transient waveforms under the TPS updating strategy with different power flows. (a) Reverse to forward power flow. (b) Forward to reverse power flow.

From (15)–(17), the transformer voltages become symmetrical over one switching period under the TPS updating strategy. Furthermore, the dc bias is eliminated. The same adjustment scheme used in the forward power flow can be applied to reverse power flow.

B. Transient Characterization With Different Power Flows

1) Reverse to Forward Power Flow: When $D_1<0<D_2$, the transient waveforms of DAB under the TPS updating strategy are shown in Fig. 6(a). Unlike the adjustment scheme in the condition of constant power flow, the phases of both the leading and lagging voltages should be adjusted. First, the phase change for the lagging voltage v_{h2} is divided into two parts according to the adjustment scheme under constant power flow. In Fig. 6(a), $\Delta t_1 = |D_1|T_{hs}$, $\Delta t_2 = D_2 T_{hs}$, $\Delta t_2' = D_2' T_{hs}$, we have

$$T_{\mathrm{hs1}}{}' = T_{\mathrm{hs1}}{}'' = T_{\mathrm{hs}} + \Delta t_2/2 = (1 + D_2/2)T_{\mathrm{hs}}. \tag{18}$$

Then, the rising edge of the leading voltage v_{h1} is also adjusted, that is,

$$\begin{cases} T'_{\mathrm{hs0}} = T_{\mathrm{hs}} + \dfrac{\Delta t_2}{2} - \Delta t_2' - \Delta t_1 \\ \qquad\quad = (1 + \dfrac{D_2}{2} - D_2' - |\,D_1|)T_{\mathrm{hs}} \\ T''_{\mathrm{hs0}} = T_{\mathrm{hs}} - \dfrac{\Delta t_2}{2} + \Delta t_2' = (1 - \dfrac{D_2}{2} + D_2')T_{\mathrm{hs}}. \end{cases} \tag{19}$$

In Fig. 6(a), the polarity of $\Delta t_2'$ is determined by $D_2{}'$. From (19), both the asymmetrical periods in (6) are also divided into two parts. According to Table I and Fig. 6(a), the HFL peak currents can also be derived

$$\begin{cases} I_1 = \dfrac{nV_2}{4f_sL}\left[(1-k)(1+D_2) + 2|\,D_1|\,k + 4D_2'k\right] \\ I_2 = \dfrac{nV_2}{4f_sL}\left[(k-1)(1-2D_2) + 2|\,D_1|\,k + 4D_2'k\right] \\ I_3 = \dfrac{nV_2}{4f_sL}\left[k - 1 - 4D_2k + 2|\,D_1|\,k + 4D_2'k\right] \\ I_4 = \dfrac{nV_2}{4f_sL} = \left[1 - k - 2D_2(k+1) + 2|\,D_1|\,k + 4D_2'k\right]. \end{cases} \tag{20}$$

Then, the dc bias $I_{T\mathrm{dc}}$ can be derived

$$I_{T\mathrm{dc}} = \frac{I_2 + I_4}{2} = \frac{nV_2}{4f_sL}(2\,|D_1\,| - 2D_2 + 4D_2')k\ . \tag{21}$$

In order to eliminate the dc bias, we set $I_{T\mathrm{dc}} = 0$, from (21),

$$D_2' = \frac{D_2 - |\,D_1|}{2}. \tag{22}$$

Combine (18) and (22), we have

$$T''_{\mathrm{hs0}} = T'_{\mathrm{hs0}} = \left(1 - \frac{|D_1|}{2}\right)T_{\mathrm{hs}}. \tag{23}$$

From (21)–(23), the transformer voltages also become symmetrical over one switching period when the power changes from the reverse to the forward power flow under the TPS updating strategy. Moreover, the dc bias is eliminated.

2) Forward to Reverse Power Flow: When $D_2 < 0 < D_1$, both the phases of the leading and lagging voltages should also be adjusted. The transient waveforms under the TPS updating strategy are shown in Fig. 6(b). First, the phase change for the lagging voltage v_{h1} is divided into two parts according to the adjustment scheme under constant power flow. In Fig. 8(b),

TABLE III
TPS SWITCHING STRATEGY AND PEAK CURRENT UNDER THE TPS UPDATING STRATEGY

Status	Power change	$T''_{hs0}=T'_{hs0}$	$T''_{hs1}=T'_{hs1}$	$D_2{}'$	$I_1/[nV_2/(4f_sL)]$	$I_2/[nV_2/(4f_sL)]$	$I_3/[nV_2/(4f_sL)]$	$I_4/[nV_2/(4f_sL)]$
Constant flow	$P\uparrow$	$1+(D_2-D_1)/2$	$2(D_2-D_1)$	$(D_1+D_2)/2$	$(1-k)(1-D_1)+(k+1)D_2$	$k-1+2D_2$	$k-1-2D_2k$	$1-k-2D_2$
	$P\downarrow$	$1+(D_2-D_1)/2$	$2(D_2-D_1)$	$(D_1+D_2)/2$				
Different flow	$-\rightarrow+$	$1-\lvert D_1\rvert/2$	$1+D_2/2$	$(D_2-\lvert D_1\rvert)/2$	$1-k+(k+1)D_2$	$k-1+2D_2$	$k-1-2D_2k$	$1-k-2D_2$
	$+\rightarrow-$	$1+\lvert D_2\rvert/2$	$1-\lvert D_1\rvert/2$	$(\lvert D_2\rvert-D_1)/2$	$1-k-(k+1)\lvert D_2\rvert$	$k-1-2\lvert D_2\rvert k$	$k-1+2\lvert D_2\rvert$	$1-k+2\lvert D_2\rvert k$

$\Delta t_1 = D_1 T_{hs}$, $\Delta t_2 = |D_2| T_{hs}$, and $\Delta t'_2 = D'_2 T_{hs}$, we have

$$T'_{\rm hs0} = T''_{\rm hs0} = T_{\rm hs} + \Delta t_2/2 = (1+|D_2\ |/2)\ T_{\rm hs}. \quad (24)$$

Then, the rising edge of the leading voltage v_{h2} is adjusted, that is,

$$\begin{cases} T'_{\rm hs1} = T_{\rm hs} + \dfrac{\Delta t_2}{2} - \Delta t'_1 = \left(1 + \dfrac{|D_2|}{2} - D'_2 - D_1\right) T_{\rm hs} \\ T''_{\rm hs1} = T_{\rm hs} - \dfrac{\Delta t_2}{2} + \Delta t'_2 = \left(1 - \dfrac{|D_2|}{2} + D'_2\right) T_{\rm hs}. \end{cases} \quad (25)$$

From (25), both the asymmetrical periods in (9) are also divided into two parts. According to Table I and Fig. 6(b), the HFL peak currents can also be derived

$$\begin{cases} I_1 = \dfrac{nV_2}{4f_sL}\left[(1-K)\left(1-|D_2|\right) - 2D_1k - 4D'_2k\right] \\ I_2 = \dfrac{nV_2}{4f_sL}\left(k - 1 - 2D_1k - 4D'_2k\right) \\ I_3 = \dfrac{nV_2}{4f_sL}\left[k - 1 + 2\,|D_2\,|(k+1) - 2D_1k - 4D'_2k\,\right] \\ I_4 = \dfrac{nV_2}{4f_sL}\left[1 - k + 4\,|D_2\,|k - 2D_1k - 4D'_2k\,\right]. \end{cases} \quad (26)$$

Then, the dc bias $I_{T\rm dc}$ can be derived

$$I_{T\rm dc} = \frac{I_2 + I_4}{2} = \frac{nV_2}{4f_sL}\ (2|\ D_2| - 2D_1 - 4D'_2)k. \quad (27)$$

In order to eliminate the dc bias, we set $I_{T\rm dc} = 0$, from (27),

$$D'_2 = \frac{|D_2| - D_1}{2}. \quad (28)$$

Combine (24) and (28), we have

$$T''_{\rm hs1} = T'_{\rm hs1} = \left(1 - \frac{D_1}{2}\right) T_{\rm hs}. \quad (29)$$

From (27)–(29), the transformer voltages become symmetrical over one switching period when the power changes from the forward to the reverse power flow under the TPS updating strategy. In addition, the dc bias is eliminated.

C. Improved Model of the Transient Process Under the TPS Updating Strategy

According to the previous analysis, the same adjustment scheme can be used for both power increase and decrease with a constant power flow; with different power flows, a different adjustment scheme should be applied in accordance with the various polarity changes. Moreover, the phases of both the leading and lagging voltages need to be adjusted.

The TPS updating strategy and the related peak currents are summarized in Table III. Unlike the transient process under the SPS updating strategy, the transformer voltages become symmetrical under the TPS updating strategy. As a result, the voltage–time product of the transformer voltages is zero during a switching period; the transient dc bias is thus eliminated.

Furthermore, the characterization of the transient process under the TPS updating strategy differs from that of the transient model in Table II. The peak currents become similar to those of the steady process in Table I after t_2 in all of the situations.

TABLE IV
TRANSIENT DC BIAS UNDER THE SPS AND TPS UPDATING STRATEGIES

		$I_{T\rm dc}/[nV_2/(4f_sL)]$		Bias polarity	
Status	Power change	SPS	TPS	SPS	TPS
Constant flow	$P\uparrow$	$2(D_2-D_1)$	0	+	–
	$P\downarrow$			–	
Different flow	$-\rightarrow+$	$2(k\lvert D_1\rvert+\lvert D_2\rvert)$	0	+	–
	$+\rightarrow-$	$-2(k\lvert D_2\rvert+\lvert D_1\rvert)$	0	–	–

V. PERFORMANCE COMPARISON OF SPS AND TPS UPDATING STRATEGIES

A. Transient DC Bias

According to the previous analysis, Table IV presents the transient dc bias under the SPS and TPS strategies. In the SPS strategy, the transient dc bias is positive when the power increases in the forward flow or changes from the reverse to the forward flow. This bias is negative when the power decreases in the forward flow or changes from the forward to the reverse flow. Moreover, the transient dc bias increases with step power. The value of the transient dc bias is mainly related to the difference between the PS ratios D_1 and D_2 with constant power flow. By contrast, that under different power flow is mainly related to the nonstrict adjustment of the PS ratios. Under the TPS strategy, the dc bias value changes to zero in all conditions.

B. Current Impact

The maximum values $I_{\rm max}$ and $\rm I_{max}$ of all peak currents are defined to characterize the current impact effects under the SPS and TPS updating strategies in the transient process,

TABLE V
COMPARISON OF CURRENT IMPACT EFFECTS BETWEEN THE SPS AND TPS UPDATING STRATEGIES

		$I_{\max}/[nV_2/(4f_sL)]$		$I'_{\max}/[nV_2/(4f_sL)]$	
Status	Power change	$k\geqslant 1$	$k<1$	$k\geqslant 1$	$k<1$
Constant flow	$P\uparrow$	$k-1-2D_1+4D_2$	$1-k-2D_1+2D_2(k+1)$	$k-1+2D_2$	$(1-k)(1-D_1)+(k+1)D_2$
	$P\downarrow$	$k-1+2D_1$	$(1-k)(1-2D_2)+2D_1$	$k-1+2D_2$	$1-k+2D_2k$
Different flow	$-\rightarrow+$	$k-1+2\lvert D_1\rvert k+4D_2$	$1-k+2\lvert D_1\rvert k+2D_2(k+1)$	$k-1+2D_2$	$1-k+(k+1)D_2$
	$+\rightarrow-$	$k-1+2D_1+2\lvert D_2\rvert(k+1)$	$1-k+2D_1+4\lvert D_2\rvert k$	$k-1+(k+1)\lvert D_2\rvert$	$1-k+2\lvert D_2\rvert k$

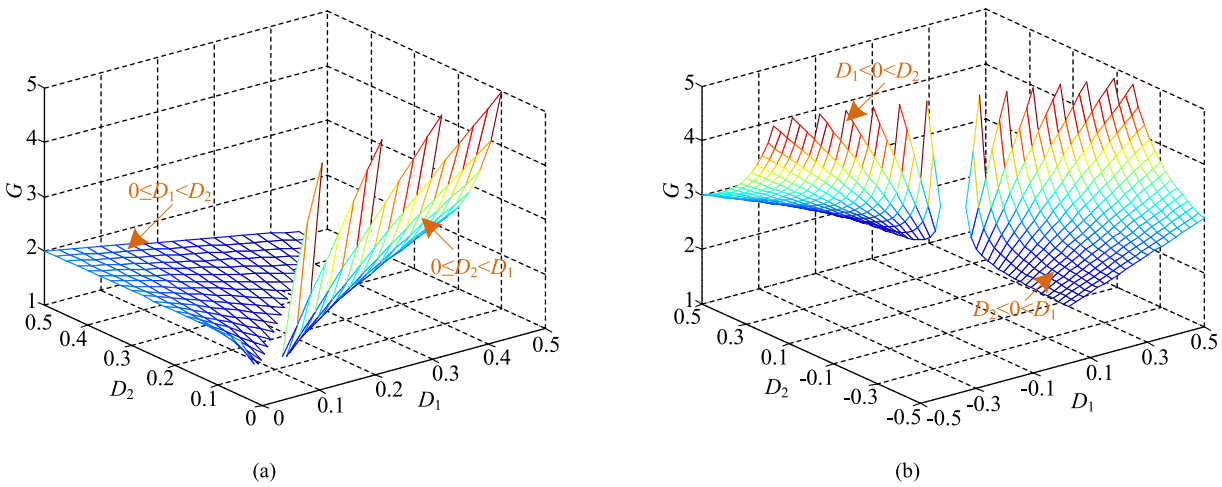

Fig. 7. Characterization of current impact. (a) Constant power flow. (b) Different power flows.

respectively; we have

$$\begin{cases} I_{\max}=\max\{I_1,I_2,I_3,I_4\} & \text{in Table II} \\ I'_{\max}=\max\{I_1,I_2,I_3,I_4\} & \text{in Table IV.} \end{cases} \tag{30}$$

From (30), $I_{\max}$ and $I'_{\max}$ can be derived as presented in Table V. When the voltage conversion ratio k varies, the maximum value changes as well. When the ratio of $I_{\max}$ and $I'_{\max}$ is employed to contrast the current impact effects of SPS and TPS, we have

$$G=\frac{I_{\max}}{I'_{\max}}. \tag{31}$$

From Table V and (31), the curves of the current impact ratio vary with the PS ratios as shown in Fig. 7. When the transient situations vary, the current impact ratio G changes as well. Nonetheless, the current impact ratio G is always greater than 1, thus indicating that the current impact of the SPS is worse than that of the TPS updating strategy in all transient processes. Given a constant power flow, G increases with the decrease in D_1 at a constant D_2 when $0\leq D_1<D_2$; G increases with D_1 at a constant D_2 when $0\leq D_2<D_1$. Given different power flows, G increases with the decrease in D_1 at a constant D_2 when $D_1<0<D_2$; G increases with D_1 at a constant D_2 when $D_2<0<D_1$. All of these variations are consistent with the change rule of the dc bias in Table IV. In Fig. 7, the voltage conversion ratio $k=1$, and the other values can be analyzed similarly.

C. Dynamic Response

According to the previous analysis, the HFL current in the transient process can be divided into ac and dc components as follows:

$$i_L(t)=i_{T\mathrm{ac}}+i_{T\mathrm{dc}} \tag{32}$$

where i_{Tac} is the same with the ac component of the steady state depicted in Fig. 1 and Table I, and $i_{T\mathrm{dc}}$ is the dc component generated by the transient dc bias.

The dynamic response time is mainly related to the decay velocity of the dc bias. It needs to be pointed out that the paper mainly discusses the performance caused by the SPS and TPS updating strategies and the response time caused by the closed-loop control parameters and the dc filter capacitor is beyond its scope. In DAB, due to the existence of the auxiliary inductance L and the coil resistance R, the dc component will attenuate exponentially with time. The mathematical model can be derived as in [26]

$$i_{T\mathrm{dc}}=I_{T\mathrm{dc}}e^{-\frac{t}{\tau}}=I_{T\mathrm{dc}}e^{-\frac{R}{\tau}t} \tag{33}$$

where $\tau=L/R$ is the decay time constant, and $I_{T\mathrm{dc}}$ is the maximum value of the dc component which is determined by the transient dc bias in Table VI.

From (33), with the same inductance and resistance, the decay velocity of the dc bias is maintained. However, because the maximum value of the dc bias is different with the different step power, the response time is also different, which increases with the increase of the step power.

TABLE VI
TPS MODULATION ALGORITHM

Transient status	$S_1/S_3 = 1, S_2/S_4 = 0$	$Q_1/Q_3 = 1, Q_2/Q_4 = 0$
$D_1 > 0$ and $D_2 > 0$	$0 \le Cnt < N$	$(N_1 + N_2)/2 \le Cnt < N_2 + N$
$D_1 < 0$ and $D_2 < 0$	$\lvert(N_1 + N_2)/2\rvert \le Cnt < N_2 + N$	$0 \le Cnt < N$
$D_1 \le 0$ and $D_2 \ge 0$	$\lvert N_1/2\rvert \le Cnt < N$	$N_2/2 \le Cnt < N + N_2$
$D_1 \ge 0$ and $D_2 \le 0$	$\lvert N_2/2\rvert \le Cnt < N + \lvert N_2\rvert$	$N_1/2 \le Cnt < N$

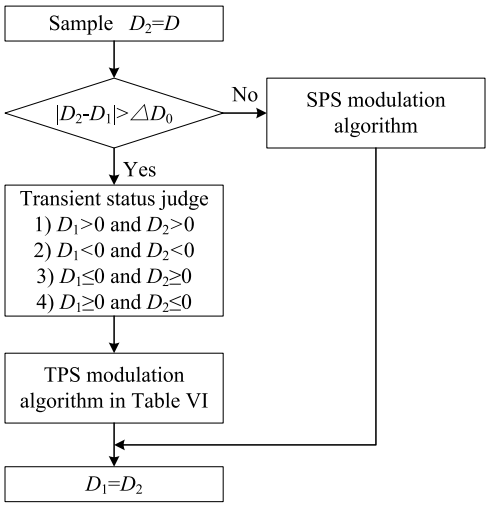

Fig. 8. TPS updating scheme.

Moreover, with the same step power, the maximum value of the dc bias is the same. However, because the decay time constant is different with different inductance, the response time is also different, which increases with the increase of the inductance. Under the TPS strategy, the HFL current can recover to the new steady state within one period because the dc bias is improved to zero. This enhancement effectively accelerates the dynamic response of the transient process.

VI. IMPLEMENTATION OF THE TPS STRATEGY IN PRACTICE

A. Modulation Implementation of the TPS Strategy

The proposed TPS control is to improve the transient dc bias and current impact, so the optimal PS is just enabled during the transient process, and the power flow control is mainly similar with the traditional SPS control.

In order to add the optimal PS during the transient process, the modulator will detect and store the PS ratios from the controller in real time, as shown in Fig. 8. When the difference between the PS ratios of the present and last periods is beyond the specifiable threshold, the modulator will judge the transient status, then the pulse width modulation (PWM) will be updated according to the different statuses in Table VI. The PS threshold can be set by the allowable safe impact current, which is usually $1.5 \sim 2I_N$.

In the TPS modulation algorithm, each switching cycle is equally discretized into 2*N* parts. The minimum discrete time

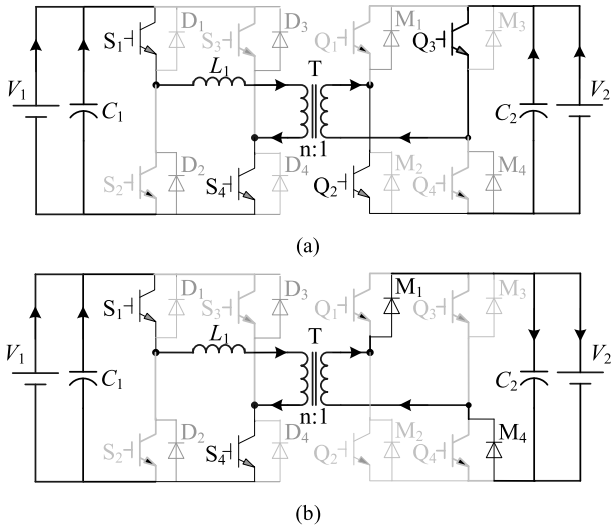

Fig. 9. Equivalent circuit when the power increases under constant flow. (a) Before t_1. (b) After t_1.

can be expressed as

$$\delta = \frac{T_{\rm hs}}{N}. \tag{34}$$

Theoretically, the modulation precision of the TPS control increases with the discretized value *N*. However, the value is limited by the operating speed of the microcontroller in practice. It is expressed as $2N \le f_{\rm cpu}/f_s$, where $f_{\rm cpu}$ is the clock frequency of the microcontroller. Using (34), the discrete amount of D_1 and D_2 can be expressed as

$$N_1 = \left[\frac{D_1 T_{\rm hs}}{\delta}\right] = [D_1 N] \tag{35}$$

$$N_2 = \left[\frac{D_2 T_{\rm hs}}{\delta}\right] = [D_2 N] \tag{36}$$

where N_1 and N_2 are the discretized values of D_1 and D_2, respectively, and the integral function $[x]$ is the function that its value is the smallest integer greater than the independent variable *x* or equal to it.

The integer variable *Cnt* is employed as a discrete counter, where $0 \le Cnt < 2N$. Then, from the previous analysis, the switching states of S_1–S_4 and Q_1–Q_4 in the TPS modulation can be expressed as in Table VI. In other instances of $0 \le Cnt < 2N$, the driving singles $S_1/S_3 = 0 S_2/S_4 = 1$ and $Q_1/Q_3 = 0 Q_2/Q_4 = 1$.

B. Dead Compensation

In the theoretical analysis presented in Sections III and IV, the dead time was not taken into account. In practice, however, the dead time $T_{\rm dead}$ must be added to prevent the shoot-through of the bridge-arm, which will cause the phase drift of DAB [9].

Here, take the constant power flow as an example to analyze. In Fig. 3(a), due to $D_2 > D_1 > 0$, thus $I_1 > 0$, before t_1, the equivalent circuit of DAB is shown in Fig. 9(a); at $t_0 + D_2 T_{hs}$, switches Q_2/Q_3 are turned off, the current flows from Q_2/Q_3 to M_1/M_4, as shown in Fig. 9(b), and the

TABLE VII
PHASE DRIFT UNDER DIFFERENT CONDITIONS

	Interval (t_1–t_0)	
Power change	SPS	TPS
$P\uparrow$	D_2T_{hs}	$\lvert D_2'\rvert T_{hs}/2$
$P\downarrow$	$\lvert D_2\rvert T_{hs}+MT_{hs}$	$\lvert D_2'\rvert T_{hs}/2$
$-\rightarrow+$	$\lvert D_2\rvert T_{hs}-MT_{hs}$	$\lvert D_2'-M\rvert T_{hs}$
$+\rightarrow-$	$\lvert D_2\rvert T_{hs}-MT_{hs}$	$\lvert D_2'-M\rvert T_{hs}$

polarity of v_{h2} changes from negative to positive immediately, thus $t_1 = t_0 + D_2T_{hs}$. The other conditions can be analyzed similarly; Table VII presents the phase drift under various conditions. When the peak currents I_0 and I_1 have the same polarity, the time interval t_1–t_0 has a drift of MT_{hs}, where $M = T_{\rm dead}/T_{hs}$ is a dead ratio. Thus, the theoretical model of the SPS strategy in Table V is offset if the dead time is disregarded except under the condition of power increase with constant flow. Based on the previous analysis, it also can be found that the drift MT_{hs} can help suppress the increase of the current impact under the SPS strategy. Moreover, the attenuation of the dc bias is accelerated. Under the TPS strategy, if the dead time is not considered, there will be a weak modulation problem in the experimental results under the conditions of different power flows.

The current offset $I_{\rm offset}$ caused by the dead drift can be derived as follows:

$$I_{\rm offset} = \frac{V_1 + nV_2}{L} MT_{\rm hs}. \tag{37}$$

To avoid weak-modulation problem of TPS, the dead compensation can be added. That is the adjustment time $\Delta t_2'$ is either decreased or increased with MT_{hs} under different conditions.

VII. EXPERIMENTAL VERIFICATION

A. Experimental Parameters

In order to verify the theoretical analysis in this paper, a DAB prototype is constructed. Both the input and output sides of the converter are connected by ac–dc PWM rectifiers to provide bidirectional power flow. The main parameters are given as follows: $P = 300\,W$, $V_1 = 106\,V$, $V_2 = 106\,V$, $L = 245\ \mu$H, $C_1 = C_2 = 450\ \mu$F, $n = 1$, and $f_s = 20$ kHz. The dead time is 0.5 μs. In the experiments, the waveforms are measured with a 500 MHz mixed signal oscilloscope MSO 4045B, the currents are measured by a high-precision ac/dc current probe TCP 305A and an amplifier TCPA 300, and the voltages are measured with a 200 MHz differential probe THDP 0200.

B. Transient Experiments Under the SPS Updating Strategy

Fig. 10 shows the transient experimental waveforms under the SPS updating strategy at constant power flow. The PS ratio increases from 0.1 to 0.3 when the power increases and it decreases from 0.3 to 0.1 when the power decreases. From Fig. 10, with the change of PS ratio, the operation waveforms of DAB are changed, which are different from the traditional principle waveforms in Fig. 1. Transient dc bias occurs in both power increase and decrease. When the power increases, the current increases in the transient process, thereby compromising the safe operation of the converter. When the power decreases, the maximum value of the HFL current is not higher than that the previous switching period. Thus, this current remains within the safe area of the converter. However, the HFL peak current also increases in comparison with that in the steady state with the same PS ratio $D = 0.1$. The increase in value can be seen from the comparison in Section VII-A.

Fig. 11 shows the transient experimental waveforms of the SPS updating strategy with different power flows. The PS ratio is changed from –0.1 to 0.3 when the power flow is changed from reverse to forward direction and from 0.3 to -0.1 when the power flow is changed from forward to reverse direction. From Fig. 11, the transient process with different power flows is similar to that with the forward and reverse power flows. Both dc bias and current impact occur in this process. However, the polarities of the transient dc bias and of current impact are similar to those of the increase and decrease states of the forward power flow when the power flow changes from reverse to forward and from forward to reverse directions, respectively. Moreover, the current impacts are higher than that in the forward and reverse power flows with the same PS ratio.

C. Transient Experiments Under the TPS Updating Strategy

The parameter changes in all of the situations under the TPS are similar to those under the SPS updating strategy; Figs. 12 and 13 show the transient experimental waveforms under the TPS updating strategy with constant and different power flows, respectively. It can be seen that the HFL currents become symmetrical, the transient dc biases are eliminated, and the current impacts are smaller than those under the SPS updating strategy in all the situations.

D. Dynamic Performance Comparison of SPS and TPS Updating Strategies

Fig. 14 shows the dynamic performance comparison of SPS and TPS updating strategies when the power changes from reverse to forward flows. The experimental parameters coincide with that in Figs. 11 and 13. Because the leading and lagging phases of the HFL voltages are exchanged between different power flows as analyzed in Section III, the HFL current are increased continually during the two adjoining switching periods, which also causes that the dc currents under the SPS strategy have larger overshoot than the TPS strategy. It also can be seen that the dynamic response is faster under the TPS strategy.

E. Comparison of the Theoretical and Experimental Results

Fig. 15 shows the comparison of the current impacts under the SPS and TPS updating strategies with constant and different power flows, respectively. In Fig. 15(a), the target PS ratio D_2 is constant at 0.24, and the initial PS ratio D_1 is changed from 0.08 to 0.24 and from 0.24 to 0.44 with an interval of 0.08 to test the power increase and decrease states with constant power flow.

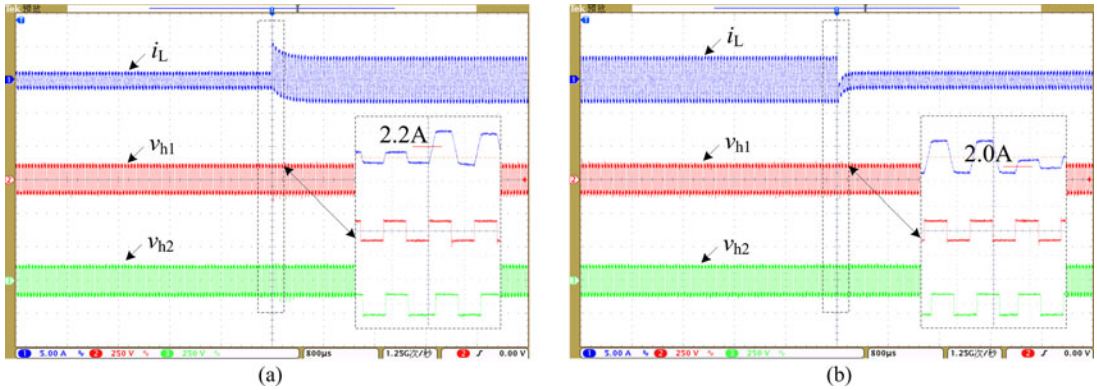

Fig. 10. Transient experimental waveforms under the SPS updating strategy with constant flow. (a) Increases in power. (b) Decreases in power.

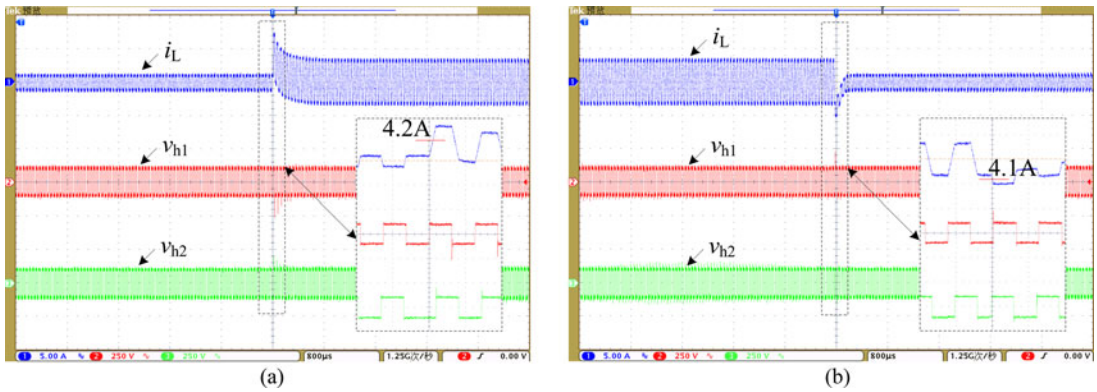

Fig. 11. Transient experimental waveforms under the SPS updating strategy with different flows. (a) From reverse to forward power flow. (b) From forward to reverse power flow.

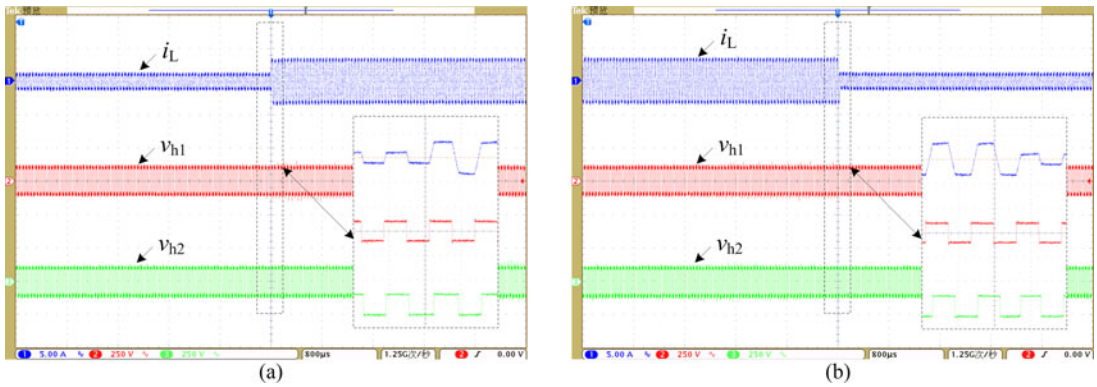

Fig. 12. Transient experimental waveforms under the TPS updating strategy with constant flow. (a) Increases in power. (b) Decreases in power.

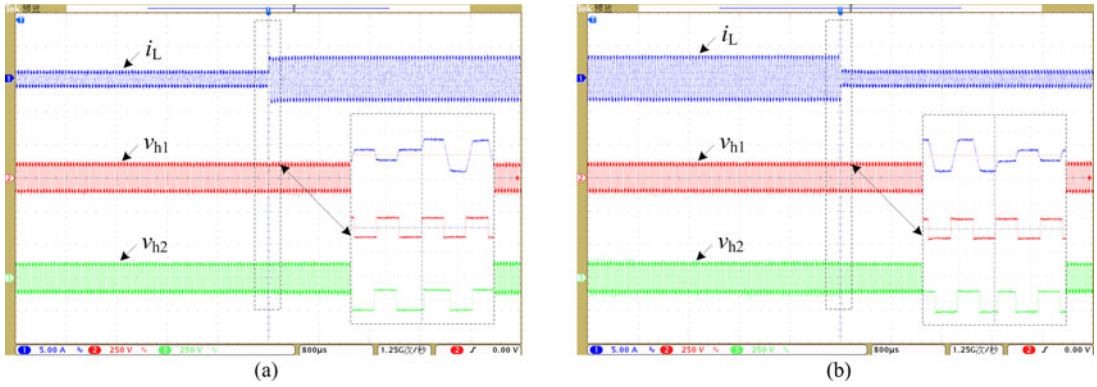

Fig. 13. Transient experimental waveforms under the TPS updating strategy with different flows. (a) From reverse to forward power flow. (b) From forward to reverse power flow.

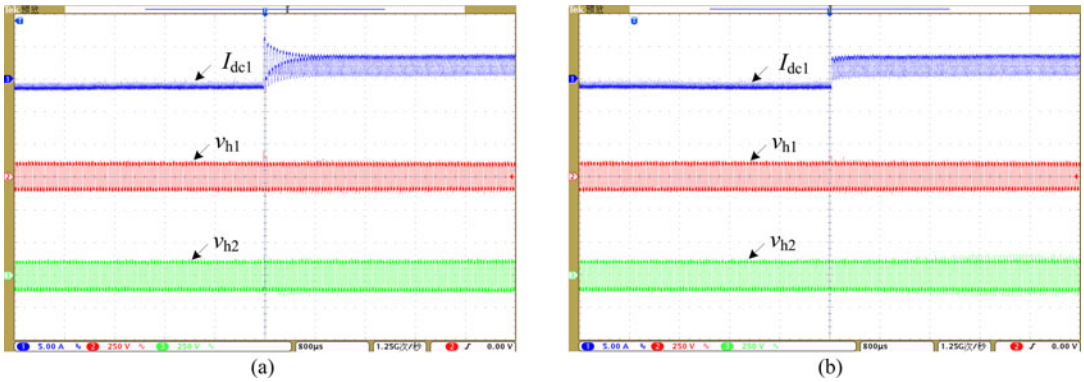

Fig. 14. Dynamic performance comparison of SPS and TPS updating strategies when the power changes from reverse to forward flow. (a) SPS. (b) TPS.

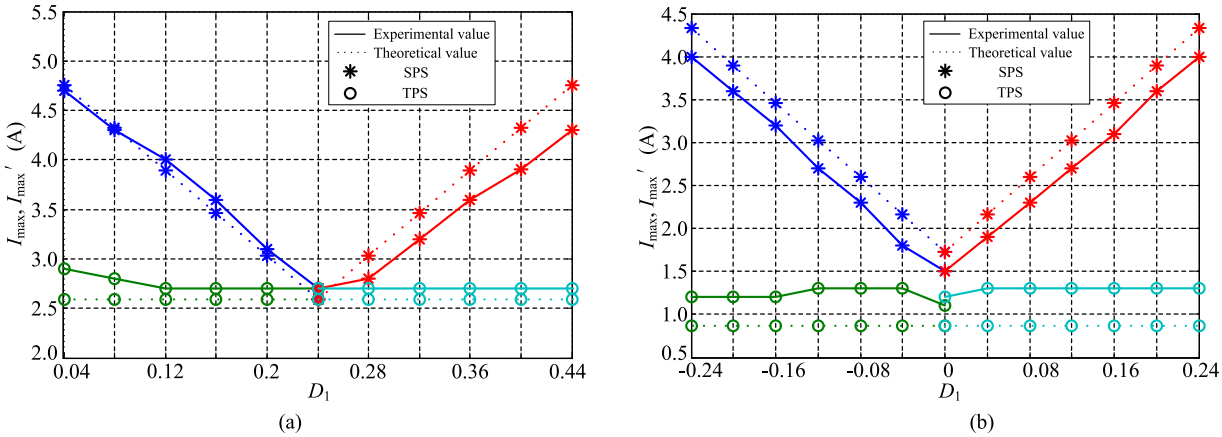

Fig. 15. Theoretical and experimental results of current impacts under SPS and TPS. (a) Constant power flow. (b) Different power flows.

In Fig. 15(b), the target PS ratio D_2 is constant at 0.08, and the initial PS ratio D_1 is changed from 0 to -0.24 with an interval of 0.08 to test the state in which the power changes from the reverse to the forward direction. Moreover, the target PS ratio D_2 is constant at -0.08, and the initial PS ratio D_1 is changed from 0 to 0.24 with an interval of 0.08 to test the state in which the power changes from the forward to the reverse direction.

From Fig. 15, for the same target PS ratio D_2 under the SPS updating strategies, the current impact varies with the different initial PS ratios. Specifically, this impact increases with the increase in the difference $|D_2 - D_1|$ in all situations. In addition, the current impacts in the TPS updating strategy are always smaller than those under the SPS updating strategies given the same parameters. Moreover, for the same target PS ratio D_2 under the TPS updating strategies, the current impacts remain almost the same given different initial PS ratios. Thus, the current impact of TPS is mainly related to the target PS ratio in the transient process.

In Fig. 15, the theoretical and experimental results are compared as well. When the power increases with constant power flow, the experimental results are consistent with the theoretical results. When the power decreases with constant power flow and when the power changes with different power flows, theoretical and experimental results display constant discrepancies. From (37), the constant error caused by dead time can be derived as $(106 + 1 * 106) * (0.5)/245 = 0.43$ A. Because the theoretical values of SPS do not take the dead time into account, the theoretical values are larger than the experimental values. Moreover, the TPS also generates the weak-modulation problem; the maximum current changes from I_1 to I_3 in Fig. 5. Hence, the experimental values in TPS are also larger than the theoretical values.

Fig. 16 shows the comparison of the theoretical and experimental results with dead compensation. It can be seen that the theoretical values of SPS are decreased and the experimental values of TPS are decreased. The experimental results agree well with the theoretical values.

According to the experimental analysis, compared to the SPS updating strategy, the TPS updating strategy eliminates the transient dc bias and improves the current impact, and further increases the response speed of the transient process effectively.

VIII. Extendibility of TPS Updating Strategies

In this paper, PS modulation is implemented by maintaining the phase of the leading voltage as a reference according to the flow direction of the power and by shifting the phase of the lagging voltage according to the magnitude of the power. But in practice, there are also other ways to implement the PS modulation, such as maintaining the phase of the lagging voltage as a reference and shifting the other phase, maintaining the phase of a fixed full-bridge as a reference and shifting the other phase, etc. Moreover, many advanced PS modulations can

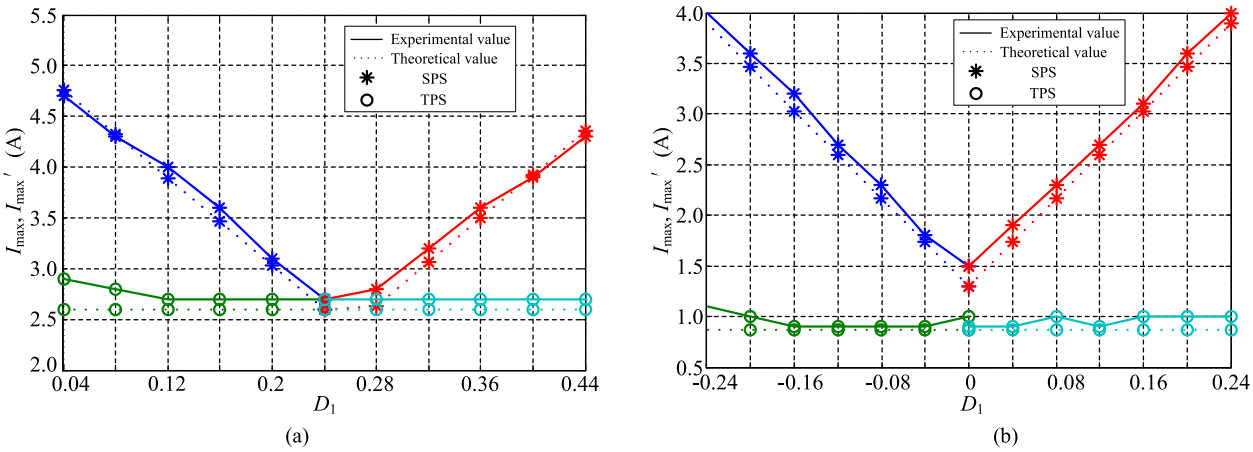

Fig. 16. Theoretical and experimental results with dead compensation. (a) Constant power flow. (b) Different power flows.

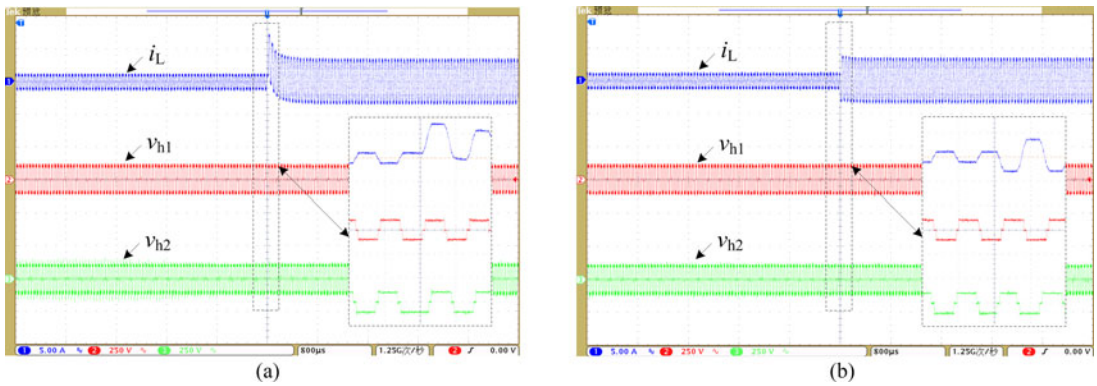

Fig. 17. Transient experimental waveforms under the SPS and TPS updating strategies with DPS modulation. (a) SPS. (b) TPS.

also be used, such as extended-PS, dual-phase-shift (DPS), etc. [8]. However, the nature of PS modulation remains the same, the transient dc bias and current impact are induced when the PS ratio is updated with the SPS strategy, and the TPS can also work.

As an extended example, Fig. 17 shows the transient experimental waveforms of the SPS and TPS updating strategies with DPS modulation. In the experiments, the inner PS ratio is 0.12; the outer PS ratio is changed from 0.1 to 0.3. It can be seen that the transient dc bias and current impact are eliminated in the DPS modulation under the TPS updating strategy. In addition, the response speed is also increased.

IX. Conclusion

In this paper, the transient dc bias and current impact effects of DAB-IBDC in practice are theoretically analyzed comprehensively and experimentally verified. Moreover, the TPS updating strategy is proposed to improve the transient performance of the traditional SPS updating strategy. According to the analysis, the characterization of the SPS updating strategy in the transient process differs from that in the steady process. The transient dc bias and current impact phenomena are induced in practice because the theoretical premise in the steady process cannot be satisfied strictly in the transient process. As a result, the safe operation of the converter is compromised. Compared to the SPS updating strategy, the TPS updating strategy eliminates the transient dc bias, improves the current impact, and further increases the response speed for all of the transient processes with constant and different power flows. The study in this paper can assist in explaining the confusing phenomena of the transient process in practice, and can recommend effective methods to engineers to improve transient performance.

References

[1] Z. Zhang, Z. Ouyang, O. C. Thomesen, and M. A. E. Andersen, "Analysis and design of a bidirectional isolated dc-dc converter for fuel cells and supercapacitors hybrid system," *IEEE Trans. Power Electron.*, vol. 27, no. 2, pp. 848–859, Feb. 2012.

[2] P. Jain, M. Pahlevaninezhad, S. Pan, and J. Drobnik, "A review of high-frequency power distribution systems: For space, telecommunication, and computer applications," *IEEE Trans. Power Electron.*, vol. 29, no. 8, pp. 3852–3863, Aug. 2014.

[3] L. Roggia, L. Schuch, J. E. Baggio, C. Rech, and J. R. Pinheiro, "Integrated full-bridge-forward dc-dc converter for a residential microgrid application," *IEEE Trans. Power Electron.*, vol. 28, no. 4, pp. 1728–1740, Apr. 2013.

[4] S. Bal, A. K. Rathore, and D. Srinivasan, "Modular snubberless bidirectional soft-switching current-fed dual 6-pack (CFD6P) dc/dc converter," *IEEE Trans. Power Electron.*, vol. 30, no. 2, pp. 519–523, Feb. 2015.

[5] F. M. Lbanez, J. M. Echeverria, J. Vadillo, and L. Fontan, "A step-up bidirectional series resonant dc/dc converter using a continuous current mode," *IEEE Trans. Power Electron.*, vol. 30, no. 3, pp. 1393–1402, Mar. 2015.

[6] Y. Xie, J. Sun, and J. S. Freudenberg, "Power flow characterization of a bidirectional galvanically isolated high-power dc-dc converter over a wide

operating range," *IEEE Trans. Power Electron.*, vol. 25, no. 1, pp. 54–66, Jan. 2010.
[7] D. Costinett, D. Maksimovic, and R. Zane, "Design and control for high efficiency in high step-down dual active bridge converters operating at high switching frequency," *IEEE Trans. Power Electron.*, vol. 28, no. 8, pp. 3931–3940, Aug. 2013.
[8] B. Zhao, Q. Song, W. Liu, and Y. Sun, "Overview of dual-active-bridge isolated bidirectional dc-dc converter for high-frequency-link power-conversion system," *IEEE Trans. Power Electron.*, vol. 29, no. 8, pp. 4091–4106, Aug. 2014.
[9] B. Zhao, Q. Song, W. Liu, and Y. Sun, "Dead-time effect of the high-frequency isolated bidirectional full-bridge dc-dc converter: Comprehensive theoretical analysis and experimental verification," *IEEE Trans. Power Electron.*, vol. 29, no. 4, pp. 1667–1680, Apr. 2014.
[10] D. Costinett, R. Zane, and D. Maksimovic, "Automatic voltage and dead time control for efficiency optimization in a dual active bridge converter," in *Proc. 27th Annu. IEEE Appl. Power Electron. Conf. Expo.*, 2012, pp. 1104–1111.
[11] H. Qin and J. W. Kimball, "Generalized average modeling of dual active bridge dc-dc converter," *IEEE Trans. Power Electron.*, vol. 27, no. 4, pp. 2078–2084, Apr. 2012.
[12] G. D. Demetriades and H. P. Nee, "Dynamic modeling of the dual-active bridge topology for high-power applications," in *Proc. IEEE Power Electron. Spec. Conf.*, 2008, pp. 457–464.
[13] X. Li and A. K. S. Bhat, "Analysis and design of high-frequency isolated dual-bridge series resonant dc/dc converter," *IEEE Trans. Power Electron.*, vol. 25, no. 4, pp. 850–862, Apr. 2010.
[14] J. H. Jung, H. S. Kim, M. H. Ryu, and J. W. Baek, "Design methodology of bidirectional *CLLC* resonant converter for high-frequency isolation of dc distribution systems," *IEEE Trans. Power Electron.*, vol. 28, no. 4, pp. 1741–1755, Apr. 2013.
[15] G. Guidi, A. Kawamura, Y. Sasaki, and T. Imakubo, "Dual active bridge modulation with complete zero voltage switching taking resonant transitions into account," in *Proc. 14th Eur. Conf. Power Electron. Appl.*, 2011, pp. 1–10.
[16] K. Wu, C. W. Silva, and W. G. Dunford, "Stability analysis of isolated bidirectional dual active full-bridge dc-dc converter with triple phase-shift control," *IEEE Trans. Power Electron.*, vol. 27, no. 4, pp. 2007–2017, Apr. 2012.
[17] H. Zhou and A. M. Khambadkone, "Hybrid modulation for dual-active-bridge bidirectional converter with extended power range for ultracapacitor application," *IEEE Trans. Ind. Appl.*, vol. 45, no. 4, pp. 1434–1442, Jul/Aug. 2009.
[18] B. Zhao, Q. Song, and W. Liu, "Efficiency characterization and optimization of isolated bidirectional dc-dc converter based on dual-phase-shift control for dc distribution application," *IEEE Trans. Power Electron.*, vol. 28, no. 4, pp. 1711–1727, Apr. 2013.
[19] G. Guidi, M. Pavlovsky, A. Kawamura, T. Lmakubo, and Y. Sasaki, "Improvement of light load efficiency of dual active bridge dc-dc converter by using dual leakage transformer and variable frequency," in *Proc. IEEE Energy Convers. Congr. Expo.*, 2010, pp. 830–837.
[20] D. Costinett, H. Nguyen, R. Zane, and D. Maksimovic, "GaN-FET based dual active bridge dc-dc converter," in *Proc. 26th IEEE Annu. Appl. Power Electron. Conf. Expo.*, 2011, pp. 1425–1432.
[21] A. Kadavelugu, S. Baek, S. Dutta, S. Bhattacharya, M. Das, A. Agarwal, and J. Scofield, "High-frequency design considerations of dual active bridge 1200V SiC MOSFET dc-dc converter," in *Proc. 26th Annu. IEEE Appl. Power Electron. Conf. Expo.*, 2011, pp. 314–320.
[22] G. Ortiz and L. Fassler, "Flux balancing of isolation transformers and application of "the magnetic ear" for closed-loop volt-second compensation," *IEEE Trans. Power Electron.*, vol. 29, no. 8, pp. 4078–4090, Aug. 2014.
[23] A. Tajfar and S. K. Mazumder, "A transformer-flux-balance controller for a high-frequency-link inverter with applications for solid-state transformer, renewable/alternative energy sources, energy storage, and electric vehicles," in *Proc. IEEE Electr. Ship Technol. Symp.*, 2011, pp. 121–126.
[24] Y. Jin, Q. Song, W. Liu, and W. Sun, "Cascaded battery energy storage system based on dual active bridges and a common dc bus," in *Proc. Int. Power Eng. Conf.*, 2011, pp. 1019–1024.
[25] X. Li and Y. F. Li, "An optimized phase-shift modulation for fast transient response in a dual-active-bridge converter," *IEEE Trans. Power Electron.*, vol. 29, no. 6, pp. 2661–2665, Jun. 2014.
[26] H. T. Tseng and J. F. Chen, "Voltage compensation-type inrush current limiter for reducing power transformer inrush current," *IET Electr. Power Appl.*, vol. 6, no. 2, pp. 101–110, Feb. 2012.

Biao Zhao (S'11–M'14) was born in Hubei, China, in 1987. He received the B.S. degree from the Department of Electrical Engineering, Dalian University of Technology, Dalian, China, in 2009, and the Ph.D. degree form the Department of Electrical Engineering, Tsinghua University, Beijing, China, in 2014, where he is currently a Postdoctoral Fellow.

His current research interests include bidirectional dc–dc converter, high-frequency-link power conversion system, and flexible dc transmission and distribution system.

Dr. Zhao is a member of the IEEE Power Electronics Society, the Industrial Electronics Society, and the Chinese Society for Electrical Engineering.

Qiang Song (M'14) was born in Changchun, China, in 1975. He received the B.S. and Ph.D. degrees from the Department of Electrical Engineering, Tsinghua University, Beijing, China, in 1998 and 2003, respectively.

He is currently an Associate Professor in the Department of Electrical Engineering, Tsinghua University. His main research interests include high power electronic interfaces for utility system, flexible ac transmission system and motor drives.

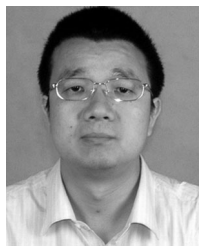

Wenhua Liu was born in Hunan, China, in 1968. He received the B.S., M.S., and Ph.D. degrees from the Department of Electrical Engineering, Tsinghua University, Beijing, China, in 1988, 1993, and 1996, respectively.

He is currently a Professor in the Department of Electrical Engineering, Tsinghua University. His main research interests include high power electronic and flexible ac transmission system.

Yuming Zhao was born in Jilin Province, China, in 1978. He received the B.S. and Ph.D. degrees from the Department of Electrical Engineering, Tsinghua University, Beijing, China, in 2001 and 2006, respectively.

He is currently a Senior Engineer (professor level) in Shenzhen Power Supply Company, Shenzhen, China. His main research interest includes dc distribution power grid.